Article

Experimental Research on Characteristics of Impulse Coupling and Plasma Plume Generated by Laser Irradiating Copper Target with Nanosecond Pulsed Laser Propulsion

Chenghao Yu [ID], Jifei Ye *, Hao Chang, Weijing Zhou, Xiao Han, Mingyu Li and Heyan Gao

State Key Laboratory of Laser Propulsion & Application, Department of Aerospace and Technology, Space Engineering University, Beijing 101416, China; yuchenghao0536@163.com (C.Y.); changhao5976911@163.com (H.C.); viviazhouyy@163.com (W.Z.); hale_1215@126.com (X.H.); merle_lee@outlook.com (M.L.); gaohy_s@163.com (H.G.)
* Correspondence: yjf1981@163.com

Abstract: The ejection of the plasma plume produced by laser ablation is an important process for inducing mechanical effects. Therefore, in this paper, the characteristics of the plasma plume are investigated in order to analyze the impulse coupling mechanism with two laser spot diameters, 300 μm and 1100 μm, respectively. The impulse generated by laser irradiating the copper target was measured by the torsion pendulum, and the plasma plume was investigated using fast photography and optical emission spectroscopy. The experimental results show that the optimal laser intensity is independent of the beam spot size. However, when the laser intensity is greater than 2.8×10^9 W/cm^2, the impulse coupling coefficient with the small beam spot starts to gradually decrease, while that with the large beam spot tends to saturate. Additionally, the stream-like structure and the semi-ellipsoid structure of the plasma plume were observed, respectively. Furthermore, the electron number density was estimated using the Stark broadening method, and the effect of the plasma plume on the impulse coupling coefficient was discussed. The results provide a technical reference for several applications including orbital debris removal with lasers, laser thrusters, and laser despinning.

Keywords: laser ablation propulsion; impulse coupling coefficient; plasma plume; fast photography; optical emission spectroscopy; electron number densities

1. Introduction

Laser ablation propulsion (LAP) shows potential solutions for many fields of growing importance, such as laser removal of orbital debris [1], laser thrusters of nano-satellites [2], and the laser despinning of non-cooperative space objects remotely [3]. LAP utilizes the recoil impulse generated by the interaction between laser and matter [4]. When an intense pulsed laser light strikes the surface of the solid target, the process of heating, melting, and vaporization occurs [5]. As the laser energy is further increased, the vapor plume is ionized and the plasma is produced. The plasma further absorbs the energy of the incident laser with near-infrared wavelength through inverse bremsstrahlung (IB) [6]. The energetic plasma plume expands rapidly away from the target surface, causing the recoil impulse to the solid target [7].

In recent years, the thrust properties generated by pulsed laser ablation of solid targets have been extensively studied [8–11]. The thrust performance of LAP is usually evaluated using the impulse coupling coefficient C_m, which is the ratio of the impulse generated by laser ablation to the incident laser energy [4]. The impulse is usually measured using the torsional pendulum [12] and the pendulum [7]. The effects of laser parameters [13], laser incidence angle [4], and material [7] on impulse coupling characteristics have been extensively investigated. As can be seen from the impulse generation process, the plasma plume characteristics have an important influence on the impulse characteristics. However,

in previous studies of laser ablation propulsion, the impulse characteristics, rather than the plume characteristics, have been the main focus. Therefore, it is necessary to investigate the plasma plume properties in combination with the impulse coupling properties. In fundamental studies of pulsed laser ablation (PLA), the plasma plumes generated by laser ablation can usually be studied using interferometry [14], a Faraday cup [15], a Langmuir probe [16], shadowgraphy [17], self-emission imaging using fast photography [18], or optical emission spectroscopy [19]. Each of the plasma plume diagnostic methods has its own characteristics. The use of multiple diagnostic methods provides a different perspective on laser-induced plasma plume characteristics and enhances the validity of the results [5].

In this study, the impulse with the laser spot diameters of 300 μm and 1100 μm was measured using the torsion pendulum, and the expansion process of the plasma plume was simultaneously visualized with fast photography and optical emission spectroscopy. The influence of the plasma plume on the impulse coupling characteristics at high laser intensity was discussed according to the plasma plume morphology. Furthermore, the electron number density was calculated by the Stark broadening method to further analyze the parameter characteristics of the plasma plume.

2. Experimental Apparatus and Methods

2.1. Apparatus

The schematic diagram of the experimental system setup is given in Figure 1. The experiment was carried out in an atmospheric environment. The experimental system was capable of measuring laser ablation impulses and simultaneously recording high-speed photographic images and emission spectra of the plasma plume. The neodymium: yttrium-aluminum-garnet (Nd: YAG) laser (Nimma-900, Beamtech Optronics, Beijing, China) with the wavelength of 1064 nm and pulse width of 8 ns was used to ablate the copper target. The radiance profile of the focused laser spot had an approximately Gaussian distribution. The pulsed laser was irradiated vertically onto the surface of the copper target through a focusing lens with a focal length of 200 mm (GCL-010154C, Daheng Optics, Beijing, China). The control of the laser spot size on the target surface was realized by changing the distance from the focusing lens to the target surface. Two typical laser spot sizes, 300 μm and 1100 μm, were selected for the experiment. The laser energy was monitored in real time during the experiment using the energy meter (FieldMax, Coherent, Santa Clara, CA, USA) to ensure the accuracy of the energy measurement.
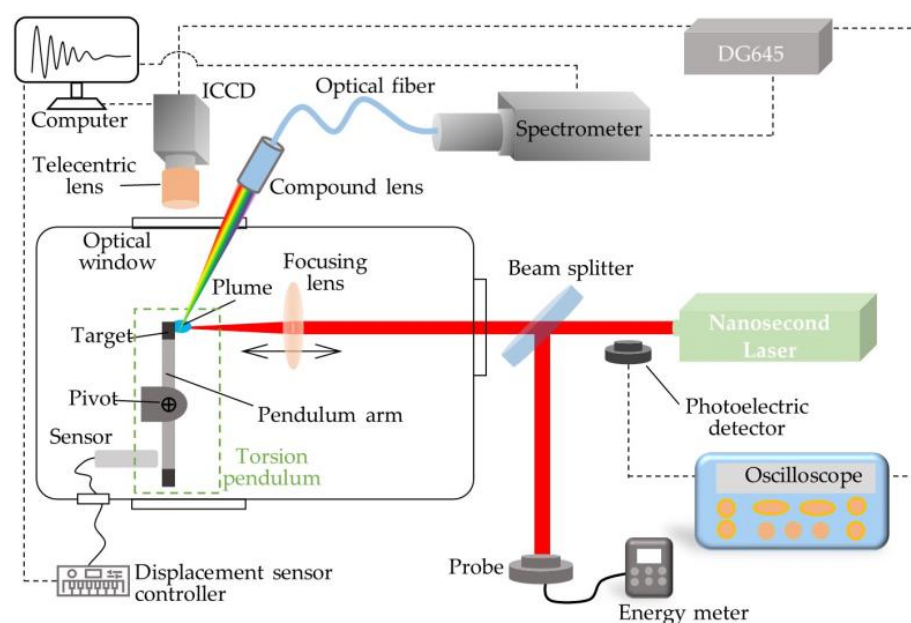

Figure 1. The schematic diagram of the experimental system.

The morphology and evolution of the plasma plume produced by laser irradiation of the copper target were visualized and recorded by ICCD camera (TRC311-S-HQB, Intelligent Scientific Systems, Beijing, China), which was positioned vertically in the direction of the plume jet. The time resolution was realized by changing the time delay between the signals in the digital delay pulse generator (DG645, Stanford Research Systems, Sunnyvale, CA, USA) that trigger the laser and the ICCD. The emission spectrum of the copper plasma was coupled into the fiber through a lens set placed at 45° normal to the target surface. Then, it was recorded by a grating spectrometer with the gratings set at 1200 groves/mm and the slit width at 20 μm. The operating timing between the laser, the ICCD camera, and the spectrometer during the experiment was coordinately controlled using the DG645.

2.2. Method of Impulse Measurement

The impulse generated by single pulse laser ablation of the copper target was measured using the torsion pendulum. After laser ablation of the copper target, the torsional motion of the torsion pendulum beam rotated around the pivot at the center caused by the impact of the impulse. The rotational angles of the torsion pendulum were measured indirectly by the displacement sensor (sensor CSE2, MICRO-EPSILON Company, Bavaria, Germany). According to the measurement principle of the torsion pendulum, the impulse I can be expressed as [20]:

$$I = \frac{J\omega_n}{L_f} \exp\left(\frac{\zeta}{\sqrt{1-\zeta^2}} \arctan \frac{\sqrt{1-\zeta^2}}{\zeta} \right) \theta_{\max}, \qquad (1)$$

where L_f represents the length of the force arm. J, ω_n, and ζ denote the rotational inertia, the intrinsic frequency, and the damping ratio of the torsion pendulum, respectively. $\Theta_{\max}$ indicates the maximum rotational angle of the torsion pendulum after laser ablation of the copper target. The detailed measurement principle of the torsional pendulum is described in the references [20–22].

2.3. Calculation Method of Electron Number Density

Electron density is an important parameter in plasma research, which helps us understand the characteristics of the plasma plume and the processes in the plasma plume. For optical thin plasmas, Stark broadening of neutral atoms or univalent ions is usually used to calculate the electron number density [23]:

$$\Delta\lambda_{1/2} = 2\omega \left(\frac{N_e}{10^{16}} \right), \qquad (2)$$

where ω is the electron collision parameter and N_e is the electron number density. $\Delta\lambda_{1/2}$ is Stark half-height full width, which can be obtained by fitting the experimental spectral data with the Lorentz function. Cu I lines, 510.6 nm $(3d^{10}(^1S)4p \rightarrow 3d^9 4s^2)$ and 521.8 nm $(3d^{10}(^1S)4d \rightarrow 3d^{10}(^1S)4p)$ were selected to calculate the N_e.

3. Results and Discussion

3.1. Ablation Impulse

The typical rotational angle of the torsion pendulum as a function of time is shown in Figure 2. According to the measurement principle of the torsion pendulum described above, the ablation impulse can be calculated from the maximum torsional angle obtained in Figure 2. The variation of the impulse generated by laser ablation of the copper target with the laser intensity in two kinds of laser spots is given in Figure 3. In each test, the target was irradiated on a single fresh location by a single pulse for impulse generation. As shown in Figure 3, the impulse increased with the laser intensity for both kinds of spot sizes. However, the influence of the spot size on the impulse was identifiable. The value of the impulse with the big beam spot was larger when the laser intensity was constant. As the laser intensity increased, the difference between the two kinds of laser beam spots became

more obvious. This is because the larger the beam spot size, the higher the single pulse laser energy with the same laser intensity. This means that more laser energy is deposited on the target, resulting in the removal of more material and stronger plume expansion. Consequently, a significantly higher ablation impulse will be generated [20].
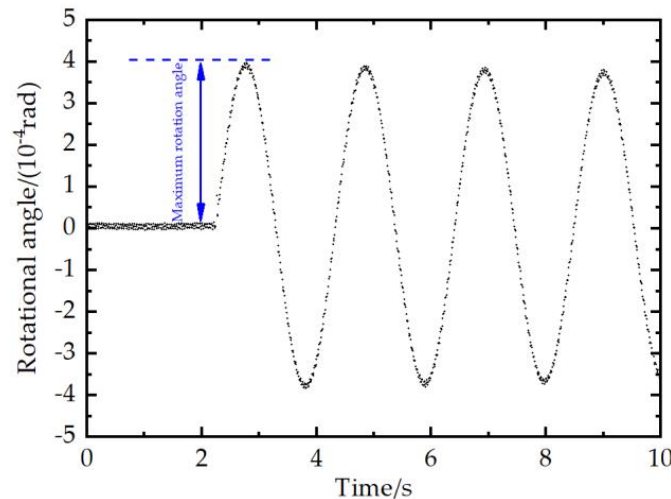

Figure 2. The typical rotational angle of the torsion pendulum as a function of time.
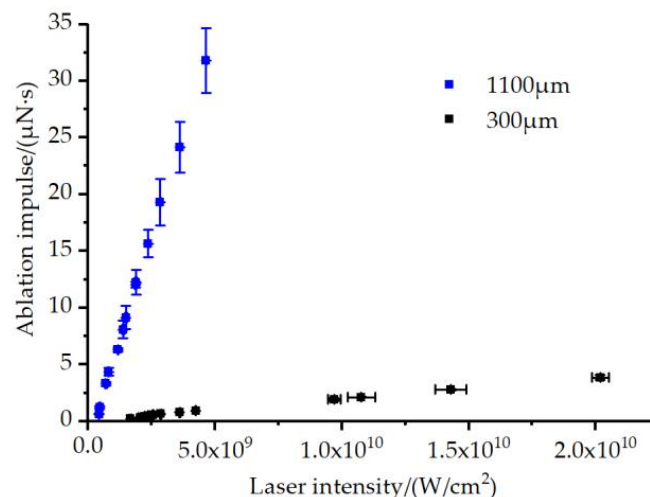

Figure 3. Variation of the ablation impulse with laser intensity in two kinds of laser spot sizes. Each experimental point in the figure represents an average of five impulse measurements. The vertical and horizontal error bars show the standard deviations of five impulse measurements and five laser intensity measurements, respectively. The length of most error bars is small. Overall, good repeatability of the experiments is demonstrated.

For evaluation of the thrust performance, the impulse coupling coefficient C_m, which is a ratio of the impulse I to the incident laser energy E ($C_m = I/E$), is commonly used. The C_m versus the laser intensity in two kinds of spot sizes are given in Figure 4a and 4b, respectively. With the increase in laser intensity, the C_m with two kinds of spot sizes first increases rapidly. When the laser intensity is much lower than 2. 8×10^9 W/cm^2, the ablation plume is dominated by the vaporization process with a lower ionization degree, resulting in poorer impulse coupling performance. As the laser intensity increases, the ablation efficiency and the ionization degree of the plume gradually increase, accompanied by the gradual improvement of the coupling performance. Therefore, the C_m increases with the increase in laser intensity and reaches the maximum value at the optimum laser intensity of about 2.8×10^9 W/cm^2. This shows that that the optimal laser intensity is independent of the beam spot size. However, the C_m at the optimal laser intensity with the

large beam spot is higher than that with the small beam spot. When the laser intensity is higher, the plasma plume formed after complete ionization of the ablation vapor absorbs the incident laser energy by inverse bremsstrahlung (IB), known as the plasma shielding effect [4]. Therefore, when the laser intensity is greater than 2.8×10^9 W/cm^2, the increase in the C_m, with the increase in the laser intensity, is hindered by the plasma shield effect. Moreover, the C_m with the small beam spot starts to gradually decrease at the higher laser intensity in Figure 4a, while the C_m with the large beam spot tends to saturate in Figure 4b.
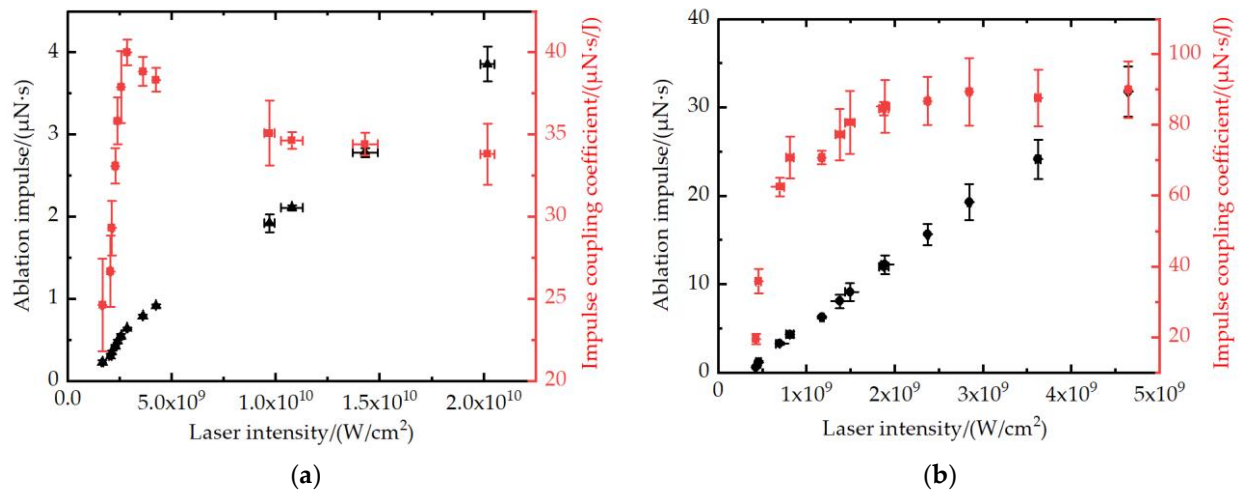

Figure 4. Variation of impulse coupling coefficient C_m with laser intensity for the laser spot diameters of (**a**) 300 μm and (**b**) 1100 μm. Every experimental data of the C_m in the figure represents the average of five calculated values. The vertical and horizontal error bars denote the standard deviations of five C_m calculations and five laser intensity measurements, respectively. There are two error sources in the calculation of the C_m, impulse error and laser intensity error, which lead to slightly larger error bars of the C_m. However, the trend of the C_m demonstrates good reproducibility.

3.2. Comparison of the Plasma Plume Image and Impulse Coupling Coefficient

The expansion of the plasma plume is the key reason for the formation of the recoil impulse on the target. Therefore, the study of the plasma plume characteristics using fast photography is conducive to revealing the impulse coupling mechanism. The fast photography can obtain two-dimensional images of the self-luminous plasma plume. The images of the plasma plume at the typical laser intensity with the spot size of 300 μm and 1100 μm are given in Figure 5a and 5b, respectively. Since the evolution of the plasma plume was around 500 ns, the gate time of the ICCD camera was set to 500 ns. As shown in Figure 5a, the morphology of the plasma plume was close to the stream-like structure with a high-radiation-intensity core and relatively dark periphery. At a laser intensity of about 10 GW/cm^2, similar stream-like structures were visualized via shadowgraph techniques by Gravel and via fast photography by Li, respectively [18,24]. Furthermore, two radiation peaks could be observed in the plasma plume image with the small spot size, which is called "plume splitting" into fast and background-slowed components [25]. The splitting plume was characterized by strong interpenetration and collision of the plasma species and background gas during plume expansion [26]. The phenomenon was greatly influenced by the presence of ionization and laser absorption in the plume. The photoionization absorption mechanism was more dominant in the region close to the target surface, but the electron–ion inverse bremsstrahlung process became more important further away from the surface [27]. As shown in Figure 5b, the plume morphology was significantly different from that with the small beam spot and was close to a semi-ellipsoidal shape. As shown in Figure 5a,b, the region of intense radiation in the plasma plume could be more obviously observed, when the laser intensity was greater than about 2.8×10^9 W/cm^2. This part consisted of a large number of ions and electrons, which absorbed a large amount of incident laser energy [28].
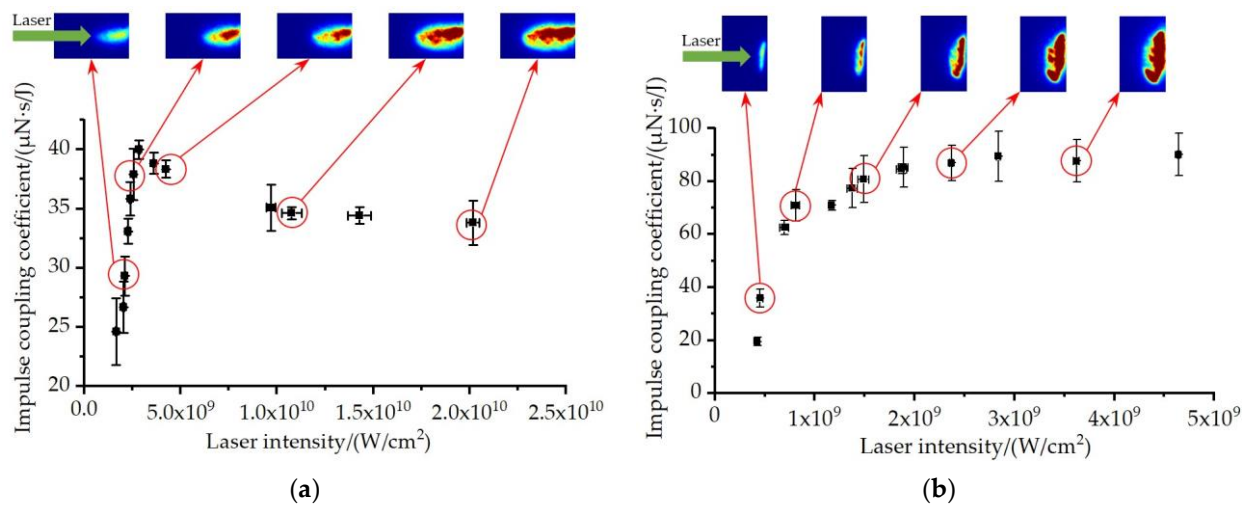
Figure 5. Plasma plume image at typical laser intensity for laser spot diameters of (**a**) 300 μm and (**b**) 1100 μm.

　　To better analyze the plasma shielding effect, time-resolved images of the plasma plume with two spot sizes at typical laser intensity were recorded in Figure 6a,b. The gate time of the ICCD camera was set to 10 ns. The time delay between the ICCD and the laser was controlled by DG645 to obtain the expansion process of the plasma plume at different times. The plasma plume emerged above the target fairly soon after the onset of the laser beam, and it could be recorded by the camera at around 10 ns before the laser reached its peak power, which was recorded as 0 ns. As shown in Figure 6a, the plasma plume expanded along the laser incidence direction and remained a stream-like structure all the time. The difference in the plume structure corresponding to the two spot sizes may be due to the enhanced plasma shielding effect caused by multi-photo ionization processes and inverse bremsstrahlung absorption [18]. In addition, the pre-ionized air channel may have provided another mechanism for the formation of the stream-like structure [29]. For the small spot size in Figure 6a, the high-energy plasma generated by laser irradiating the copper target produced particles with faster longitudinal velocities via absorbing more laser energy. In Figure 6a, the plasma plume lasted about 300 ns. In the first 10 ns, the plasma plume expanded rapidly and basically reached the maximum plume size at about 10 ns. The front expansion velocity could be dramatically accelerated by dynamic source and partial ionization effects in the direction perpendicular to the target surface at early times [30]. The interaction of accelerated and stationary ions through multi-encounter Coulomb scattering may have contributed to the phenomenon of accelerated expansion [31]. Since the expansion of the plasma plume was accelerated mainly in the perpendicular direction, it became more nonsymmetric and forward peaked [30]. In addition, the highest radiation intensity region was mainly distributed along the laser incidence direction, rather than the target surface, which is evidence of the enhanced plasma shielding effects. The distributions of the plasma for the small laser spot might have increased the optical path length of the laser in plasma and altered the energy absorption structure. Most of the laser energy would have been absorbed by the plasma plume, other than that which was delivered to the surface of copper target. Therefore, when the laser intensity was greater than 2.8×10^9 W/cm^2, the LAP thrust performance for the small spot was reduced, accompanied by the reduced C_m due to the enhanced plasma shielding effect. Furthermore, it can be seen that the plasma plume front at 10 ns to 140 ns basically remained unchanged with the high radiation intensity. After 200 ns, the radiation intensity of the plasma plume gradually diminished due to the collision with air molecules and to radiative cooling.
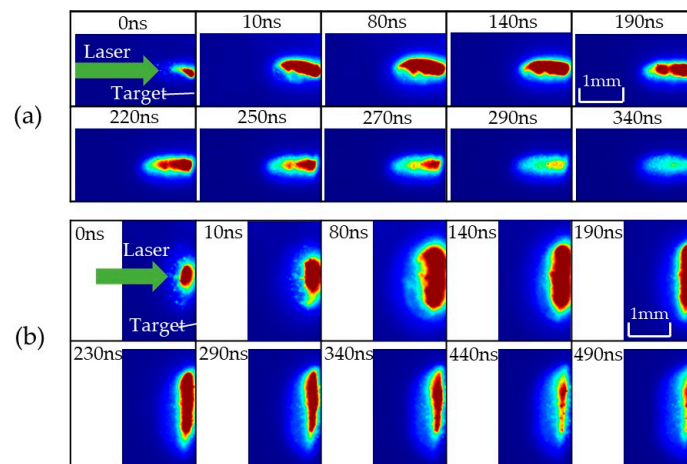
Figure 6. When the laser intensity was 4×10^9 W/cm^2, the evolution process of the plasma plume at the spot diameters of (**a**) 300 μm and (**b**) 1100 μm.

As shown in Figure 6b, for the first 10 ns, the plasma plume expanded rapidly. The plume expanded in the direction of laser incidence and parallel to the target surface simultaneously. For the large spot size of 1100 μm, the high density of electrons and ions in the plasma plume were mainly distributed along the direction parallel and close to the target surface. The distance of the incident laser passing through the high-density plasma region was relatively shorter compared to the small spot size. Therefore, when the laser intensity was greater than 2.8×10^9 W/cm^2, the large spot reduced the plasma shielding effect and improved thrust performance. The difference between the plasma distribution in the plume with the two spot sizes had an important influence on the impulse coupling characteristics. Furthermore, the plume size reached its maximum at about 80 ns. After 140 ns, the plume size decreased along the laser incidence direction, but remained unchanged along the parallel direction of the target surface. This was caused by the fact that the plasma expanded faster along the laser incident direction, while the plasma expanded slower along the parallel direction of the target surface. After 190 ns, the radiation intensity of the plasma plume decreased rapidly with the increase in time.

3.3. Optical Emission Spectroscopy

The study of electron number density in plasma plumes is helpful to analyze the coupling mechanism of pulsed laser ablation impulses. The spectrometer was started from the moment of pulse laser light output, and the gate width was set to 1 μs. Figure 7 shows the change of emission spectra of copper plasma with time for two spot sizes. As shown in Figure 7a, the spectral line width with the small spot did not decrease pronouncedly from 500 ns to 2000 ns. However, in Figure 7b, the spectral line width with the large spot clearly decreased from 500 ns to 2000 ns, indicating that the electron number density obviously decreased. Furthermore, the emission spectrum intensity with the large spot did not decrease significantly during this period, which was the result of complex interactions among the excited plasma components [18].
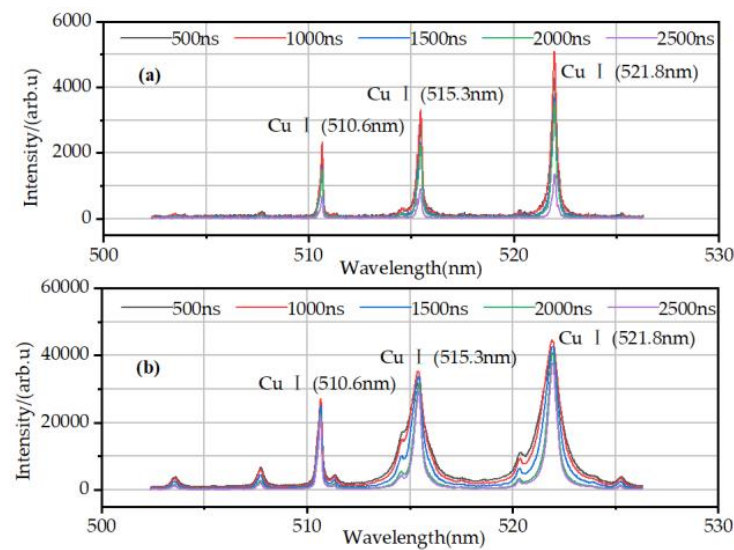
Figure 7. When the laser intensity was 4×10^9 W/cm^2, the evolution process of the emission spectra at the spot diameters of (**a**) 300 μm and (**b**) 1100 μm.

According to the Stark broadening method, the electron number density N_e could be estimated from the emission spectral lines obtained experimentally. The trend of the N_e over time for the two spot sizes is shown in Figure 8. It can be seen that the N_e with the large laser spot is always higher than that with the small laser spot. When the laser intensity was constant, the single pulse energy with the large spot was higher than that with the small spot, resulting in more laser energy coupled with the copper target. The larger laser energy vaporized and ionized more target materials initially. Therefore, the N_e of the plasma plume was higher with the large spot. This resulted in the stronger jet of the plasma plume and the larger ablation impulse corresponding to the large spot. Furthermore, the N_e of the two kinds of laser spots decreased with the increase in time. The difference was that the N_e with the small beam spot decreased more slowly with time. The long-lasting high-density plasma absorbed the subsequent laser energy, preventing it from reaching the surface of the copper target. Therefore, the impulse coupling performance of the small beam spot decreased at higher laser intensity. This provides further evidence of the enhanced plasma shielding effect.
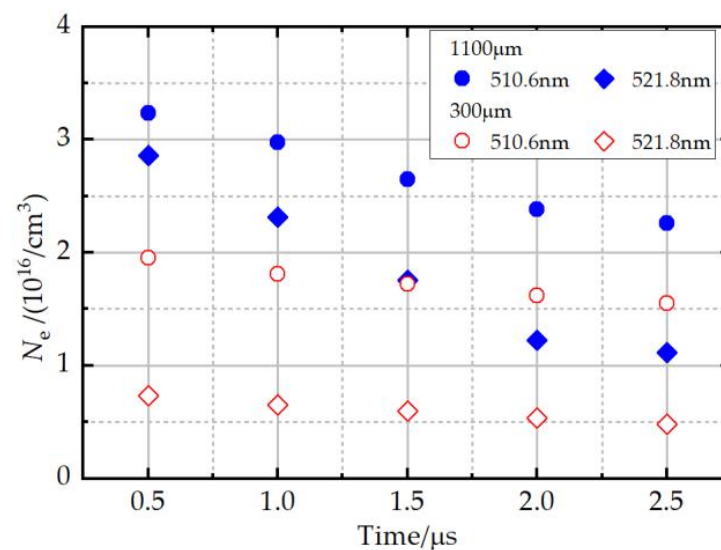

Figure 8. When the laser intensity was 4×10^9 W/cm^2, the electron number density N_e varied with time in two spot sizes.

4. Conclusions

In this paper, the impulse generated by ablating the copper target with different laser intensities for two different spot sizes was measured using the torsion pendulum. Simultaneously, the plasma plume was investigated using fast photography and emission spectroscopy. When the laser intensity was constant, the ablation impulse of the large laser spot was greater than that of the small spot, resulting from more energy deposition. As the laser intensity increased, the difference in impulse between the two spot sizes became more obvious. At high laser intensity, the C_m with the small beam spot started to gradually decrease, while the C_m with the large beam spot tended to saturate. In addition, the difference in the plasma distribution in the plume with the two spot sizes had an important influence on the impulse coupling characteristics. The morphology of the plasma plume with the small beam spot was close to the stream-like structure, while that with the large beam spot was close to the semi-ellipsoidal shape. For the small laser spot, the distribution of the plasma increased the optical path length of the laser in plasma and altered the energy absorption structure, which greatly suppressed the subsequent laser ablation of the copper target via an enhanced shielding effect. Furthermore, the electron number density estimated by the Stark broadening of the lines was larger in the case of large spot sizes, consistent with the greater impulse measured by the torsion pendulum. To sum up, the role played by the laser beam size in determining the characteristics of impulse coupling and plasma plume will be of importance in several applications, including orbital debris removal with lasers, laser thrusters, and laser despinning.

Author Contributions: Conceptualization, C.Y. and J.Y.; methodology, H.C.; software, W.Z.; investigation, M.L.; resources, H.G.; data curation, C.Y.; writing—original draft preparation, C.Y.; writing—review and editing, J.Y.; visualization, X.H.; supervision, J.Y.; funding acquisition, H.C and W.Z. All authors have read and agreed to the published version of the manuscript.

Data Availability Statement: The data presented in this study are available on request from the corresponding author. The data are not publicly available due to privacy restrictions.

Conflicts of Interest: The authors declare no conflict of interest.

References

1. Phipps, C.R. L'ADROIT—A Spaceborne Ultraviolet Laser System for Space Debris Clearing. *Acta Astronaut.* **2014**, *104*, 243–255. [CrossRef]
2. Phipps, C.R.; Luke, J.R.; Lippert, T.; Hauer, M.; Wokaun, A. Micropropulsion Using Laser Ablation. *Appl. Phys. A* **2004**, *79*, 1385–1389. [CrossRef]
3. Kumar, R.; Sedwick, R.J. Despinning Orbital Debris Before Docking Using Laser Ablation. *J. Spacecr. Rockets* **2015**, *52*, 1129–1134. [CrossRef]
4. Wang, B. Laser Ablation Impulse Generated by Irradiating Aluminum Target with Nanosecond Laser Pulses at Normal and Oblique Incidence. *Appl. Phys. Lett.* **2017**, *110*, 014101. [CrossRef]
5. Hussein, A.E.; Diwakar, P.K.; Harilal, S.S.; Hassanein, A. The Role of Laser Wavelength on Plasma Generation and Expansion of Ablation Plumes in Air. *J. Appl. Phys.* **2013**, *113*, 143305. [CrossRef]
6. Breitling, D.; Schittenhelm, H.; Berger, P.; Dausinger, F.; Hügel, H. Shadowgraphic and Interferometric Investigations on Nd:YAG Laser-Induced Vapor/Plasma Plumes for Different Processing Wavelengths. *Appl. Phys. A Mater. Sci. Process.* **1999**, *69*, S505–S508. [CrossRef]
7. Zhao, X.; Tang, F.; Han, B.; Ni, X. The Influence of Laser Ablation Plume at Different Laser Incidence Angle on the Impulse Coupling Coefficient with Metal Target. *J. Appl. Phys.* **2016**, *120*, 213103. [CrossRef]
8. Sinko, J.E.; Phipps, C.R. Modeling CO_2 Laser Ablation Impulse of Polymers in Vapor and Plasma Regimes. *Appl. Phys. Lett.* **2009**, *95*, 131105. [CrossRef]
9. Tran, D.; Yogo, A.; Nishimura, H.; Mori, K. Impulse and Mass Removal Rate of Aluminum Target by Nanosecond Laser Ablation in a Wide Range of Ambient Pressure. *J. Appl. Phys.* **2017**, *122*, 233304. [CrossRef]
10. Phipps, C.; Birkan, M.; Bohn, W.; Eckel, H.-A.; Horisawa, H.; Lippert, T.; Michaelis, M.; Rezunkov, Y.; Sasoh, A.; Schall, W.; et al. Review: Laser-Ablation Propulsion. *J. Propuls. Power* **2010**, *26*, 609–637. [CrossRef]

11. Yu, C.; Ye, J.; Zhou, W.; Chang, H.; Guo, W. Micro-Impulse and Plasma Plume Produced by Irradiating Aluminum Target with Nanosecond Laser Pulses in Double-Pulse Scheme. *Plasma Sci. Technol.* **2022**, *24*, 074009. [CrossRef]
12. Tsuruta, H.; Wang, B.; Wang, Z.; Yokota, S.; Sasoh, A. Repetitive Pulse Performance of One-Micrometer Laser-Ablation Propulsion onto Aluminum. *J. Propuls. Power* **2014**, *30*, 1485–1489. [CrossRef]
13. Zhang, N.; Wang, W.; Zhu, X.; Liu, J.; Xu, K.; Huang, P.; Zhao, J.; Li, R.; Wang, M. Investigation of Ultrashort Pulse Laser Ablation of Solid Targets by Measuring the Ablation-Generated Momentum Using a Torsion Pendulum. *Opt. Express* **2011**, *19*, 8870–8878. [CrossRef] [PubMed]
14. Wei, W.; Li, X.; Wu, J.; Yang, Z.; Jia, S.; Qiu, A. Interferometric and Schlieren Characterization of the Plasmas and Shock Wave Dynamics during Laser-Triggered Discharge in Atmospheric Air. *Phys. Plasmas* **2014**, *21*, 083112. [CrossRef]
15. Sankar, P.; Shashikala, H.D.; Philip, R. Effect of Laser Beam Size on the Dynamics of Ultrashort Laser-Produced Aluminum Plasma in Vacuum. *Phys. Plasmas* **2019**, *26*, 013302. [CrossRef]
16. Anoop, K.K.; Polek, M.P.; Bruzzese, R.; Amoruso, S.; Harilal, S.S. Multidiagnostic Analysis of Ion Dynamics in Ultrafast Laser Ablation of Metals over a Large Fluence Range. *J. Appl. Phys.* **2015**, *117*, 083108. [CrossRef]
17. Mori, K.; Maruyama, R.; Shimamura, K. Energy Conversion and Momentum Coupling of the Sub-KJ Laser Ablation of Aluminum in Air Atmosphere. *J. Appl. Phys.* **2015**, *118*, 073304. [CrossRef]
18. Li, X.; Wei, W.; Wu, J.; Jia, S.; Qiu, A. The Influence of Spot Size on the Expansion Dynamics of Nanosecond-Laser-Produced Copper Plasmas in Atmosphere. *J. Appl. Phys.* **2013**, *113*, 243304. [CrossRef]
19. Smijesh, N.; Rao, K.H.; Chetty, D.; Litvinyuk, I.V.; Sang, R.T. Plasma Plumes Produced by Laser Ablation of Al with Single and Double Pulse Schemes. *Opt. Lett.* **2018**, *43*, 6081–6084. [CrossRef]
20. Zhou, W.; Chang, H.; Ye, J.; Li, N. Impulse of Planar and Sphere Target by Nanosecond Laser Ablation in a Large Beam Spot. *Laser Phys.* **2020**, *30*, 066002. [CrossRef]
21. Zhou, W.-J.; Hong, Y.-J.; Chang, H. A MicroNewton Thrust Stand for Average Thrust Measurement of Pulsed Microthruster. *Rev. Sci. Instrum.* **2013**, *84*, 125115. [CrossRef] [PubMed]
22. Yu, C.; Zhou, W.; Chang, H.; Chen, Y. Experimental Research on Impulse Coupling Characteristics and Plasma Plume Dynamics of a Nanosecond Pulsed Laser Irradiated Aluminum Target. *IEEE Access* **2020**, *8*, 205272–205281. [CrossRef]
23. Haq, S.U.; Ahmat, L.; Mumtaz, M.; Shakeel, H.; Mahmood, S.; Nadeem, A. Spectroscopic Studies of Magnesium Plasma Produced by Fundamental and Second Harmonics of Nd:YAG Laser. *Phys. Plasmas* **2015**, *22*, 083504. [CrossRef]
24. Gravel, J.-F.Y.; Boudreau, D. Study by Focused Shadowgraphy of the Effect of Laser Irradiance on Laser-Induced Plasma Formation and Ablation Rate in Various Gases. *Spectrochim. Acta Part B At. Spectrosc.* **2009**, *64*, 56–66. [CrossRef]
25. Wood, R.F.; Chen, K.R.; Leboeuf, J.N.; Puretzky, A.A.; Geohegan, D.B. Dynamics of Plume Propagation and Splitting during Pulsed-Laser Ablation. *Phys. Rev. Lett.* **1997**, *79*, 1571–1574. [CrossRef]
26. Han, M.; Gong, Y.; Zhou, J.; Yin, C.; Song, F.; Muto, N.; Takiya, T.; Iwata, Y. Plume Dynamics during Film and Nanoparticles Deposition by Pulsed Laser Ablation. *Phys. Lett. A* **2002**, *302*, 182–189. [CrossRef]
27. Chen, Z.; Bogaerts, A. Laser Ablation of Cu and Plume Expansion into 1atm Ambient Gas. *J. Appl. Phys.* **2005**, *97*, 063305. [CrossRef]
28. Marla, D.; Bhandarkar, U.V.; Joshi, S.S. Critical Assessment of the Issues in the Modeling of Ablation and Plasma Expansion Processes in the Pulsed Laser Deposition of Metals. *J. Appl. Phys.* **2011**, *109*, 021101. [CrossRef]
29. Panchenko, A.N.; Shulepov, M.A.; Tel'minov, A.E.; Zakharov, L.A.; Paletsky, A.A.; Bulgakova, N.M. Pulsed IR Laser Ablation of Organic Polymers in Air: Shielding Effects and Plasma Pipe Formation. *J. Phys. Appl. Phys.* **2011**, *44*, 385201. [CrossRef]
30. Chen, K.R.; Leboeuf, J.N.; Wood, R.F.; Geohegan, D.B.; Donato, J.M.; Liu, C.L.; Puretzky, A.A. Accelerated Expansion of Laser-Ablated Materials near a Solid Surface. *Phys. Rev. Lett.* **1995**, *75*, 4706–4709. [CrossRef]
31. Koopman, D.W. Momentum Transfer Interaction of a Laser-Produced Plasma with a Low-Pressure Background. *Phys. Fluids* **1972**, *15*, 1959–1969. [CrossRef]